



# Structural and magneto-transport features of cobalt-substituted mixed-valence manganites

Sevgi Polat Altintas<sup>1,\*</sup>

<sup>1</sup>Department of Physics, Bolu Abant İzzet Baysal University, 14030 Bolu, Turkey

**Received:** 7 December 2020

**Accepted:** 28 January 2021

**Published online:**  
15 February 2021

© The Author(s), under exclusive licence to Springer Science+Business Media, LLC part of Springer Nature 2021

## ABSTRACT

We report the results of a detailed investigation of the role of cation substitution Co → Mn on the structural, microstructural, magnetic, and transport properties of the manganite system  $\text{La}_{2/3}\text{Ca}_{1/3}\text{Mn}_{1-x}\text{Co}_x\text{O}_3$  ( $x = 0.0, 0.1, 0.2$  and  $0.3$ ). It is found that the replacement of Mn with Co does not change the crystal structure of the parent compound  $\text{La}_{2/3}\text{Ca}_{1/3}\text{MnO}_3$  which crystallizes in orthorhombic structure with Pbnm space group. From a systematic analysis of the magneto-transport measurements, it has been shown that the cobalt substitution leads to a decrease in the system magnetization and lowering of Curie and metal-insulator transition temperatures. The magnetoresistance percentage (MR%), which is found to change significantly by Co substitution and exceeds 100% for  $x = 0.3$  sample at low temperatures, is also reported at 1 T applied magnetic field.

## 1 Introduction

Investigation of the role of the transition element doping of the cobaltites and manganese oxides with perovskite structure has received extensive attention, recently [1–20]. The subject, indeed, promises an in-depth understanding of the fundamental condensed matter physics and its technological prospective applications for current and near-future technologies. The compounds with formulas  $\text{LaMnO}_3$  and  $\text{LaCoO}_3$  are examples of such perovskite structures that exhibit insulator and antiferromagnetic properties at room temperature due to the absence of  $\text{Mn}^{4+}$  and  $\text{Co}^{4+}$  ions, respectively [21, 22]. On the other hand, substituting the divalent elements, such as Sr, Ca, and Ba, instead of  $\text{La}^{3+}$  ions can lead to trivalent Mn or Co

ions to be converted to a mixture of  $\text{Mn}^{3+}$  and  $\text{Mn}^{4+}$  or  $\text{Co}^{3+}$  and  $\text{Co}^{4+}$  [1, 2]. Recent studies have shown a phase transition from an insulating phase to the ferromagnetic metallic one as a function of the increasing inverse temperature, which is caused by the substituting  $\text{La}^{3+}$  ions by  $\text{Sr}^{2+}$  ones [1–4]. This phase transition is signaled by a sharp change in the resistivity of the considered compounds. However, we would like to stress here that the physical mechanisms that explain the magnetoresistance effects for these oxides are quite different. While in the manganite system, the existence of ferromagnetism and the metallic behavior is attributed to the double-exchange (DE) interaction between  $\text{Mn}^{3+}$  and  $\text{Mn}^{4+}$  ions [23–25], and strong electron–phonon interaction arising from the Jahn–Teller splitting plays a crucial

Address correspondence to E-mail: sevgialtintas@ibu.edu.tr

role in the observed colossal magnetoresistance (CMR) effect [26, 27], the observed exotic features in the hole-doped lanthanum-based cobaltites arise from their additional spin and lattice degrees of freedom. More explicitly, cobalt ions may possess either high, intermediate, or low-spin states depending on the temperature of the environment, which strongly affects the magneto-electrical properties of the system.

The perovskite structures have the general formula  $ABO_3$  where A and B indicate metallic cations and O is a nonmetallic anion [23, 24]. Recently, the A-site of manganese perovskites has been substituted by various rare earth and alkaline earth elements which were shown to lead to several unusual features in the properties of the resulting compounds [6, 19, 28–32]. In B-site substitution, manganese is, generally, replaced by transition elements. Since Mn ions play a key role in the magnetoresistance of manganites, the substitution of B-site with transition metals is a very effective way of tailoring the magnetic properties of  $LaMnO_3$ . In recent years, particular transition elements, such as Ti, Cr, Fe, Co, and Cu, were used as dopants in manganites [1, 12, 33–35]. Doping in the B-site causes substantial changes in the  $Mn^{3+}-O-Mn^{4+}$  chain and leads to irreversible interactions among the Mn ions and the transition element. In this kind of substitution, the  $Mn^{3+}/Mn^{4+}$  ratio can change substantially in the manganese sublattice which can affect the magnetic and electrical features and create structural inhomogeneities in the sample [12, 34, 36].

In the present study, we aim to investigate the manganite system  $La_{2/3}Ca_{1/3}Mn_{1-x}Co_xO_3$  ( $x = 0.0, 0.1, 0.2, \text{ and } 0.3$ ). Among the other transition elements, cobalt substitution is expected to have a special effect due to the possession of prominently different electron configuration and spin states from Mn [1–4]. Co doping is expected to lead to substantial changes in the crystalline and the magneto-electric properties. We have carried out an extensive experimental study of the effect of the amount of cobalt doping on the structural, microstructural, electric, and magnetic properties. We have found that Co substitution leads to a marked reduction in the Curie and the metal–insulator transition temperatures and a decrease in the spontaneous magnetization. We also show that 30% of substituted Co can significantly enhance the magnetoresistance of the considered manganite system at low temperatures.

## 2 Experimental

The manganites formulated as  $La_{2/3}Ca_{1/3}Mn_{1-x}Co_xO_3$  with  $x = 0.0, 0.1, 0.2, \text{ and } 0.3$  were prepared using the traditional solid-state reaction method. The powders  $La_2O_3$ ,  $CaCO_3$ ,  $CoO$ , and  $MnO_2$  were selected to have purity higher than 99.9% which were mixed in stoichiometric ratios, ground, and then calcined at temperature 1173 K for 20 h. The obtained black powder was further ground by using pestle and mortar. The resulting powder was pelletized and then sintered for 20 h at temperature 1273 K with two intermediate grindings. As a final procedure, the resultant pellets are reground, further pelletized, and then annealed for 24 h at temperature 1423 K. To avoid the formation of oxygen vacancies, all pellets were left to be furnace-cooled down to room temperature. Hereafter, the studied samples will be called as C0, C1, C2, and C3 for  $x = 0.0, 0.1, 0.2, \text{ and } 0.3$ , respectively. To examine the crystal structure and the phase purity, we employed powder X-ray diffraction (XRD) method which uses a Rigaku Multiflex diffractometer with  $CuK_\alpha$  radiation at wavelength  $\lambda = 1.5418 \text{ \AA}$ . Diffractograms were arranged to measure  $2\theta$  angle values in the range  $20^\circ$ – $80^\circ$  by using  $0.004^\circ$  step size with a 3 s per step. The Rietveld method in JANA2006 software was used to refine the phase structure of the measured X-ray data [37]. Scanning electron microscope (SEM) (code: JEOL 6390-LV) was used to investigate the microstructure of the samples. The resistivity of the samples is measured using the traditional four-probe method on a He gas contact cryocooler and superconducting coil magnet over a temperature range between 50 and 300 K. The response of the sample resistivity to the applied magnetic field (which was set 1 T) is indicated by the quantity named as the magnetoresistance percentage (MR%) which is given by the following formula:

$$MR \% = [(R_0 - R_H)/R_0] \times 100, \quad (1)$$

where  $R_H$  ( $R_0$ ) is the measured resistance under 1 T (0 T) magnetic field. The magnetization measurements of samples were performed under 50 Oe applied field with a 7304 model Lake Shore Vibrating Sample Magnetometer (VSM) under zero-field-cooled mode.

### 3 Results and discussion

#### 3.1 Structure and morphology

We have performed powder X-ray diffraction measurements to analyze the structural phase characterization of the considered compounds. The diffraction patterns are shown in Fig. 1. We also make an enlargement of the most intense peaks for higher visibility in the inset of Fig. 1. The powder X-Ray diffraction patterns indexed in an orthorhombic-distorted perovskite-type structure with ( $N^{\circ}62$ ) space group over the whole doping concentration range [13, 38]. In Fig. 2, we demonstrate the Rietveld-refined XRD patterns of the samples, and the structural parameters are tabulated in Table 1. We would like to remark here that the observed XRD patterns and the calculated one through Rietveld refinement are in good agreement based on discrepancy factor as Goodness of Fit (GOF) and Reliability factors ( $R_p$  and  $R_{wp}$ ) shown in Table 1. One may conclude here that the samples of interest have a single-phase. The XRD peaks are relatively sharp and have a high intensity which shows that the compounds of interest are deeply crystalline. From the Rietveld-refined analysis, there are no observed impurity peaks indicating lanthanum or manganese oxide phases through the experimental accuracy limits.

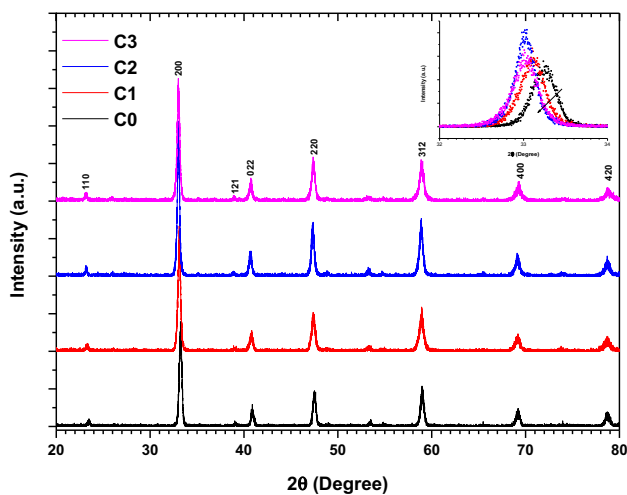


**Fig. 1** (Color online) X-ray powder diffraction patterns for  $\text{La}_{2/3}\text{Ca}_{1/3}\text{Mn}_{1-x}\text{Co}_x\text{O}_3$ . Here the lines colored as (black, red, blue, magenta) correspond to  $x = (0.0, 0.1, 0.2, 0.3)$  samples, respectively. The inset demonstrates the shift in the most intense peaks due to variation in the Co doping concentration

From the XRD analysis, it is also found that the lattice parameters slightly change with the increase in cobalt content. This results in a slight cell volume increase as a function of the amount of Co doping, except  $x = 0.2$  sample (see Table 1). The unit cell volume increase can be also justified from the diffraction peaks in the inset of Fig. 1. The peaks shift to the lower  $2\theta$  values as the Co content increases which shows the signatures of the enhancement in the unit cell parameters [39]. The radius of the substituted elements and the concentrations of the  $\text{Mn}^{3+}$  and  $\text{Mn}^{4+}$  ions are different which can be considered as the main reasons for the shifts in the diffraction peaks. Like manganese, cobalt can be found in the perovskite structure in various valences and spin states [40]. The spin states of  $\text{Co}^{2+}$ ,  $\text{Co}^{3+}$ , and  $\text{Co}^{4+}$  ions can be found in a high or a low state. There can be a random distribution of Mn and Co ions in the lattice which is the main reason for the slight cell volume increase [18]. For example, the ionic radius of  $\text{Co}^{2+}$  ion in the high-spin (HS) state is larger than the ionic radius of  $\text{Mn}^{3+}$  ion in the HS state and  $\text{Mn}^{3+}$  ions can be replaced by  $\text{Co}^{2+}$  ions. Also, it is expected that  $\text{Mn}^{4+}$  ions can be replaced by  $\text{Co}^{3+}$  ions in the low-spin (LS) state. Thus, the reason for the slight increase in unit cell volume with increasing cobalt content may be confirmed with this assertion (see Table 2 for ionic radii of Mn and Co cations).

It is important to analyze the microstructure of the samples since it gives insights into the effect of structural aspects such as grain size and porosity on the features of the manganites. For that purpose, we use scanning electron microscopy (SEM) techniques to investigate the microstructure and morphology of the considered samples. The results are presented in Fig. 3. The morphology of the samples is seen to be composed of polycrystalline microstructure in which the manganite particles are almost uniform and have relatively fine grains. Moreover, from the SEM images, we observe almost spherically shaped grains with inhomogeneous size distribution. It seems that the Co substitution leads to agglomeration with varying degrees. Using Gaussian fitting method [42], average particle sizes are estimated which decreases from 1.28  $\mu\text{m}$  for  $x = 0.0$  sample to 0.93  $\mu\text{m}$  for  $x = 0.3$  sample.

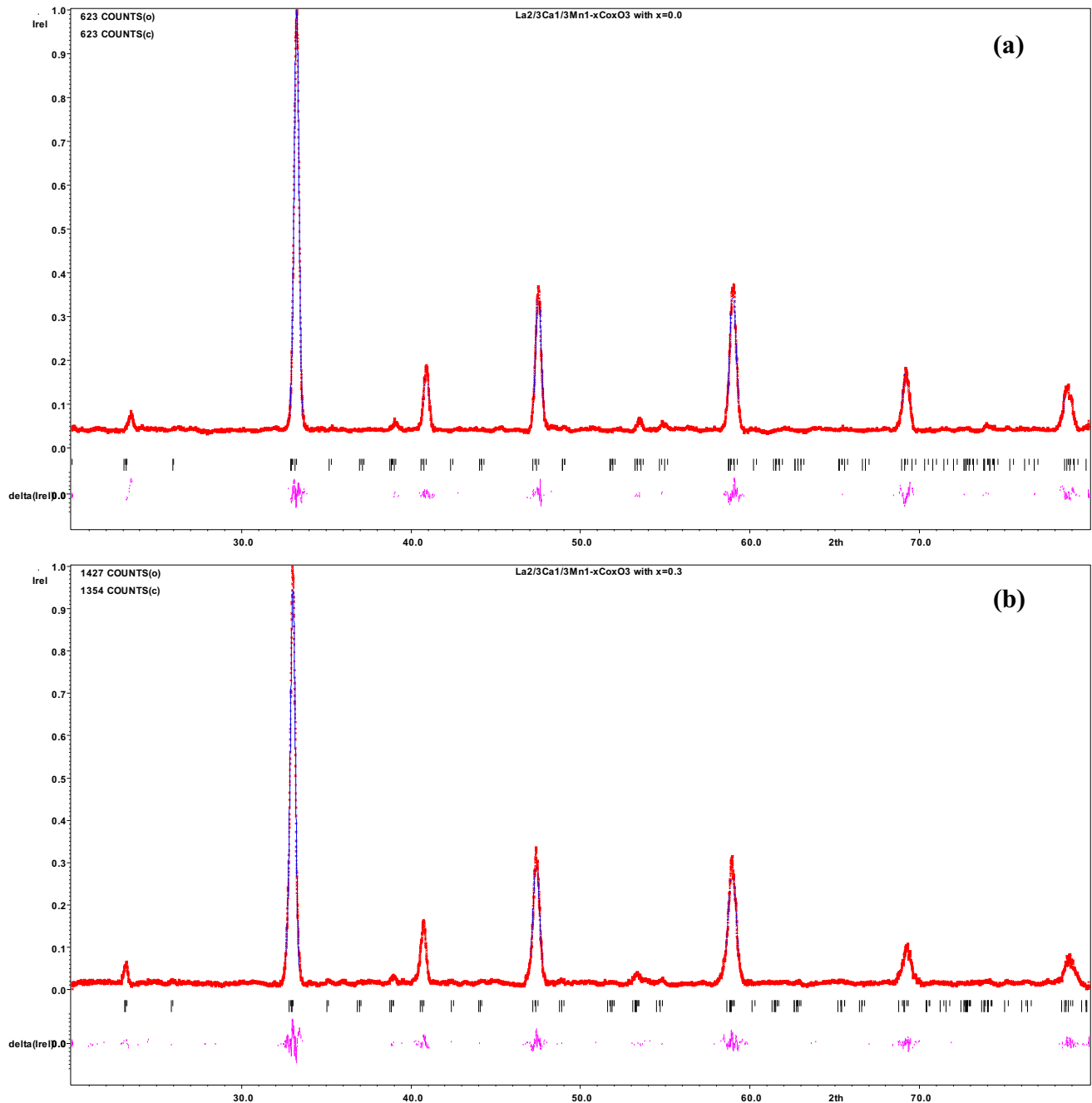


**Fig. 2** (Color online) Rietveld refinement powder XRD patterns for **a**  $\text{La}_{2/3}\text{Ca}_{1/3}\text{MnO}_3$  and **b**  $\text{La}_{2/3}\text{Ca}_{1/3}\text{Mn}_{0.7}\text{Co}_{0.3}\text{O}_3$ . The red cross line shows the experimental data, while the blue solid line demonstrates the calculated pattern. The black ticks represent the

positions of the Bragg reflections for the main phase. The magenta line at the bottom shows the difference between the experimental and the calculated patterns

### 3.2 Magneto-electrical properties

In Fig. 4, we depict the magnetization as a function of the temperature for the samples of interest in a fixed magnetic field at 50 Oe. We observe sharp drops in the magnetization as a function of the temperature

which indicates the magnetic transitions in the samples. This also verifies here that the samples have high homogeneity as mentioned above in the XRD measurement analysis. The sharp changes in the magnetization elucidate the phase transition from the ferromagnetic regime to the paramagnetic regime

**Table 1** Lattice parameters  $a$ ,  $b$ , and  $c$  (in units of Å), the volume of the unit cell (in units of Å<sup>3</sup>), and the refinement parameters for La<sub>2/3</sub>Ca<sub>1/3</sub>Mn<sub>1-x</sub>Co<sub>x</sub>O<sub>3</sub> with  $x = 0.0, 0.1, 0.2,$  and  $0.3$  samples which are obtained from the Rietveld refinement analysis of the powder XRD patterns

$x$	0.0	0.1	0.2	0.3
Space group	Pbnm (N°62)			
La <sub>2/3</sub> Ca <sub>1/3</sub> Mn <sub>1-x</sub> Co <sub>x</sub> O <sub>3</sub>				
$a$ (Å)	5.4425	5.4581	5.4537	5.4553
$b$ (Å)	5.4012	5.4162	5.4120	5.4304
$c$ (Å)	7.6994	7.6561	7.6592	7.6741
$V$ (Å <sup>3</sup> )	226.3347	226.3361	226.0712	227.3461
GOF	0.42	0.83	0.86	0.95
$R_p$	5.13	9.14	8.52	9.97
$R_{wp}$	7.03	12.75	12.13	14.58

where the transition temperature is known as the Curie temperature ( $T_C$ ). The minimum of the derivative  $dM/dT$  can be used to determine the Curie temperature which is drawn for the undoped sample in the inset of Fig. 4 and tabulated in Table 3 for all samples. It is obvious from Fig. 4 and Table 3 that the cobalt substitution results in a decrease both in the system magnetization and in the Curie temperature. This is expected since the Co doping decreases the LCMO ferromagnetic ratio. As a further explanation, the double-exchange interaction is controlled by Mn<sup>3+</sup> and Mn<sup>4+</sup> ions which determine  $T_C$  in the La<sub>1-x</sub>Ca<sub>x</sub>MnO<sub>3</sub> system [23–25]. By cobalt doping, Mn<sup>3+</sup> ions are partially replaced by Co atoms which can weaken the double-exchange interaction between Mn<sup>3+</sup> and Mn<sup>4+</sup> ions. This results in a decrease both in the magnetization and the Curie temperature [1, 4]. The decrease of the magnetization,  $M$ , at low temperatures ( $< 100$  K) for the C2 and C3 samples is due to magnetic inhomogeneities that are attributed to the strong competitions between the ferromagnetic double-exchange and antiferromagnetic superexchange (phase separation) interactions [2]. In Table 3, the transition widths  $\Delta T_C$ , which are the value of the full

width at half maximum of the  $dM/dT$  peaks (see the inset of the Fig. 4), are also tabulated which decreases as the function of the amount of Co content indicating the sharp phase transition as a function of temperature.

Now we investigate the effect of Co substitution on the parameter, the so-called, electrical resistivity at different temperatures. From such an analysis, one can determine the effect of doping on the possible transition between metallic and insulator phases and the critical temperature in which the phase transition occurs. Therefore, in Fig. 5, we depict the temperature dependence of the resistivity for the samples with and without Co substitution. It is clear from the figure that the Co substitution significantly increases the resistivity of the samples. However, the increase in resistivity has no linear dependence on the amount of Co substitution at a given temperature. Please remark here that the increase (decrease) in the resistivity with the increase in the temperature is the indication of the metallic (insulator) phase. We report here that for all samples, both phases exist. For the compounds with  $x = 0.0, 0.1,$  and  $0.2,$  there is one characteristic (peak) temperature  $T_p$  that highlights the metal–insulator transition. For the temperatures below  $T_p$ , the resistivity increases as a function of temperature indicating the metallic phase. On the other hand, for the temperatures  $T > T_p$  the samples have an insulating phase. It is obvious from the figure (also from Table 3) that the characteristic temperature substantially decreases as the amount of Co substitution increases. An interesting result is obtained for the 30% Co substitution case in which we report two characteristic temperatures  $T_{p1}$  and  $T_{p2}$  as labeled in Fig. 5 (see also Table 3) [15, 43]. Between  $T_{p1}$  and  $T_{p2}$ , the sample has both an insulator and metallic phases. The low-temperature metal–insulator transition at  $T_{p2}$  for the C3 sample is related to the granular nature of the ceramics and can be explained as follows: The considered ceramic manganite sample is composed of two phases: the grain inside as the bulk phase, and the grain boundary regions as the

**Table 2** Ionic radii (Å) of Mn and Co cations [41]

Coordination	Mn <sup>3+</sup>		Mn <sup>4+</sup>		Co <sup>2+</sup>		Co <sup>3+</sup>		Co <sup>4+</sup>	
	HS	LS	HS	LS	HS	LS	HS	LS	HS	LS
VI	0.645	0.58	0.53		0.745	0.65	0.61	0.542	0.53	–



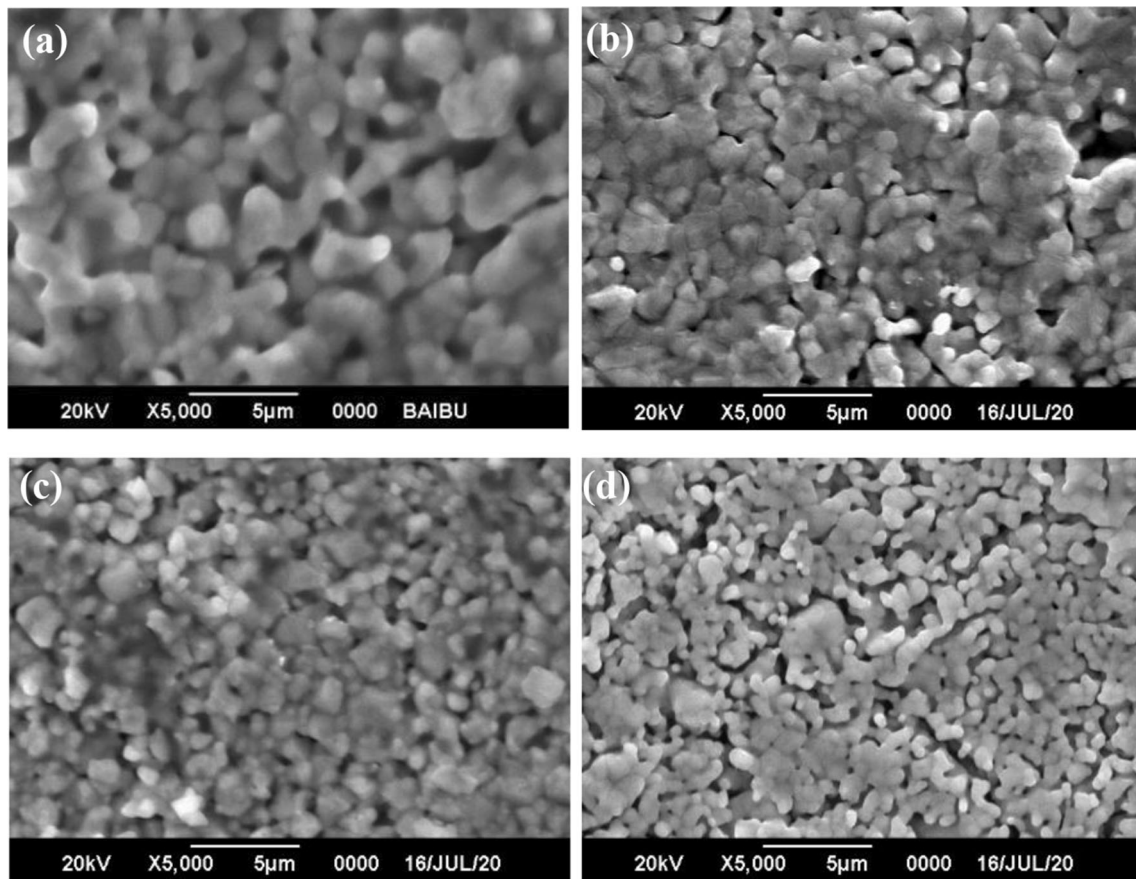


**Fig. 3** Scanning electron microscopy (SEM) micrographs of  $\text{La}_{2/3}\text{Ca}_{1/3}\text{Mn}_{1-x}\text{Co}_x\text{O}_3$  with  $x = 0.0$  (a), 0.1 (b), 0.2 (c), and 0.3 (d)

**Fig. 4** (Color online) Magnetization versus the temperature for the samples  $\text{La}_{2/3}\text{Ca}_{1/3}\text{Mn}_{1-x}\text{Co}_x\text{O}_3$  with  $x = 0.0, 0.1, 0.2,$  and  $0.3$ . The inset shows the phase transition temperature,  $T_C$ , for the parent sample, i.e.,  $x = 0.0$

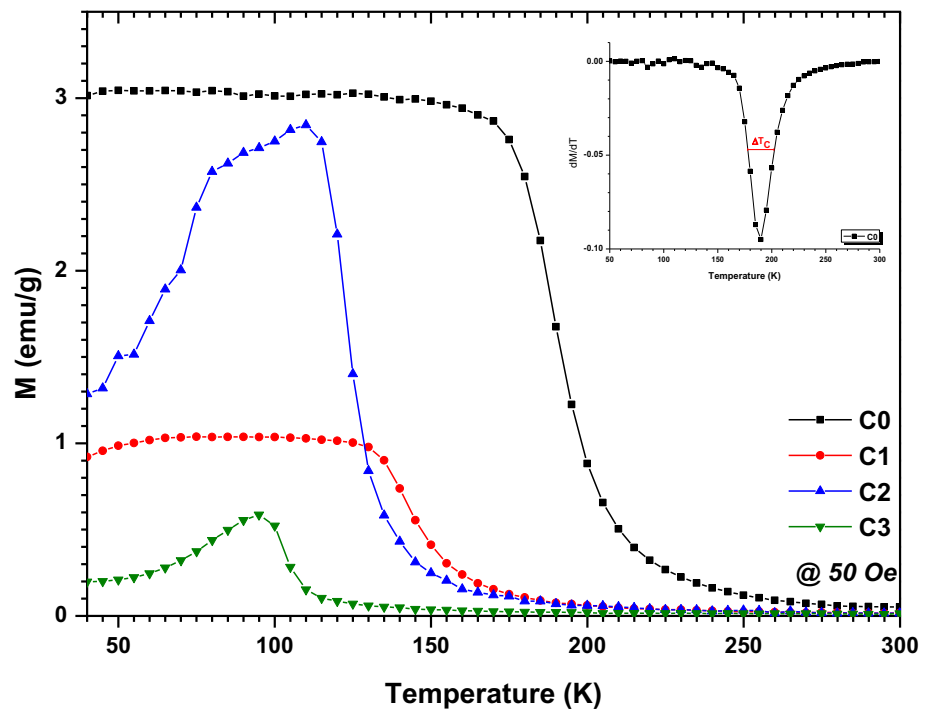


**Table 3** Experimental parameters obtained from  $M(T)$  and  $\rho(T)$  data for the samples  $\text{La}_{2/3}\text{Ca}_{1/3}\text{Mn}_{1-x}\text{Co}_x\text{O}_3$  with  $x = 0.0, 0.1, 0.2,$  and  $0.3$

Parameters (K)	$x = 0.0$	$x = 0.1$	$x = 0.2$	$x = 0.3$
$T_C$	190	140	123	104
$\Delta T_C$	25.9	22.8	16.6	12.2
$T_{P1}$	201	160	38	116
$T_{P2}$	–	–	–	54

All the parameters are explained in the text

surface phase. Hence two electrical transport processes are in competition: the bulk one similar to that in the single crystals (corresponding to  $T_{P1}$  which is near  $T_C$  and is in accordance with our results in the  $M(T)$  curve) and the intergranular transport through the surface phase of the grains corresponding to the  $T_{P2}$  at a lower temperature [44]. In comparison to the undoped sample ( $x = 0.0$ ), the characteristic temperature shifts to the smaller values for 30% Co-substituted sample. The change in the resistivity and  $T_P$  for the Co-substituted samples can be interpreted as follows. The introduced Co ions perturb the  $\text{Mn}^{3+}$ – $\text{O}$ – $\text{Mn}^{4+}$  network which can reduce the available states for hopping. The interaction in the network is weakened by the Co ions which can decrease the

conductivity and the characteristic temperature [10, 11].

Now we investigate how the external magnetic field affects the resistivity of the considered samples at different temperatures. In Fig. 6, we plot the magnetoresistance percentage (MR%) versus temperature under 1 T applied magnetic field. Please recall here the formula of the magnetoresistance percentage which is given as  $\text{MR}\% = [(R_0 - R_H)/R_0] \times 100$ . The negative MR% values indicate the enhancement of the sample resistivity under the applied magnetic field. High absolute MR% values are desirable for the technological applications which demonstrate a strong response of the sample resistivity to the applied magnetic field [45, 46]. For the sample without Co substitution, we report positive MR% values for the all considered temperature range. This indicates the reduction of the resistivity under 1 T magnetic field. Approximately, 60% MR value can be obtained around 190 K. For the 10% Co-substituted sample, we have positive MR% values which are less in contrast to the undoped sample one. The MR% values range approximately between 5 and 20% and do not show any appreciable dependencies on the temperature. For the 20% Co substitution, even the 1 T magnetic field has no pronounced effect on the resistivity for the temperatures approximately lower than 130 K; the sample resistivity can be increased by the field for the temperatures higher

**Fig. 5** (Color online) The temperature dependence of the electrical resistivity for the samples  $\text{La}_{2/3}\text{Ca}_{1/3}\text{Mn}_{1-x}\text{Co}_x\text{O}_3$  with  $x = 0.0, 0.1, 0.2,$  and  $0.3$ . The inset shows an expanded view for the C0 resistivity curve (black line in the main figure)

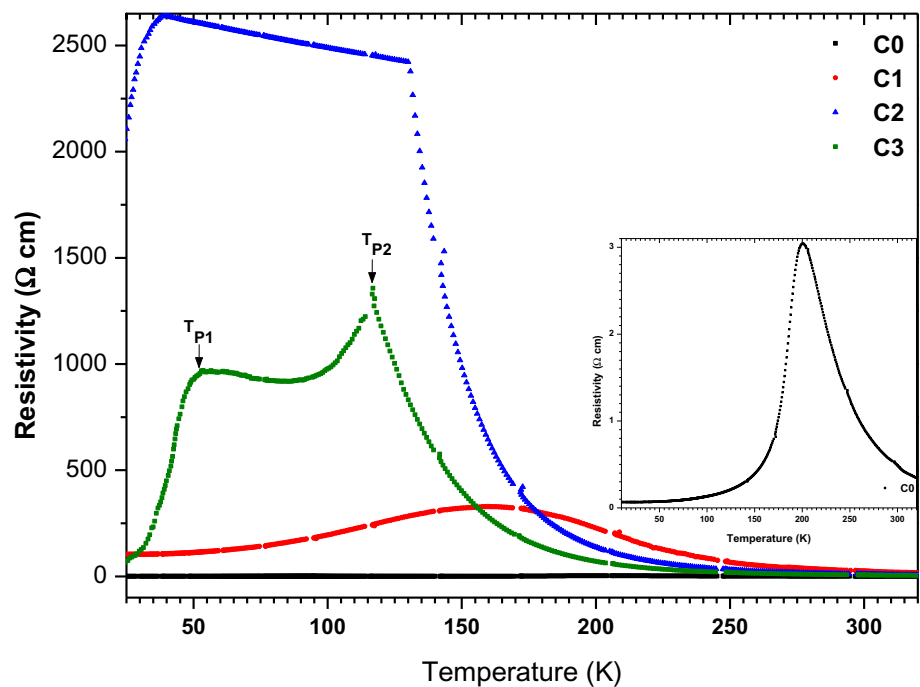
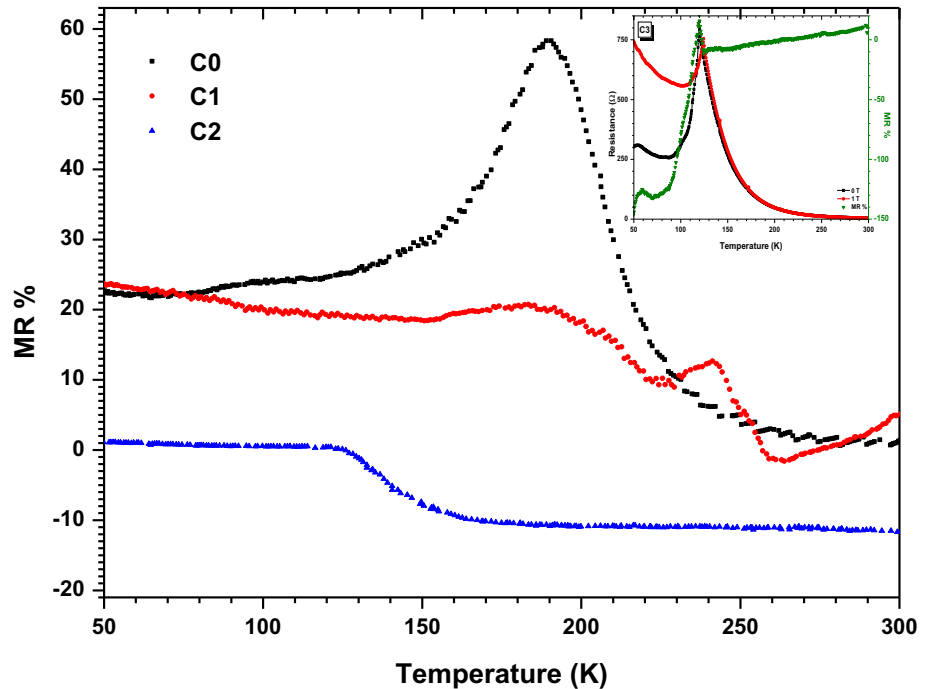


**Fig. 6** (Color online) The calculated temperature-dependent MR% values for the samples  $\text{La}_{2/3}\text{Ca}_{1/3}\text{Mn}_{1-x}\text{Co}_x\text{O}_3$  with  $x = 0.0, 0.1,$  and  $0.2$  under 1 T applied magnetic field. The inset shows the temperature dependence of the resistance for  $x = 0.3$  sample at zero and 1 T magnetic field and MR% value versus temperature



than 130 K. This is indicated by the negative MR% values as shown by the blue triangular line in Fig. 6. However, the negative MR% values are almost the same at different temperatures for the 20% Co-substituted sample. A remarkable result is obtained for the 30% Co substitution. The absolute MR% values can be higher than 100% for the temperatures smaller than 100 K (see the inset in Fig. 6). In other words, at low temperatures, there is a significant increase in the resistivity under the external magnetic field. On the other hand, the resistivity for the 30% Co-substituted sample can also exhibit reduction under the field at high temperatures ( $T > 200$  K) as noted by the positive MR% values (approximately 10%) in the inset. The sign of MR% changes from negative to positive values when the temperature is increased above the Curie temperature,  $T_C$ . At high temperatures above  $T_C$ , the magneto-transport properties are primarily determined by the conduction of lattice polarons, while at low temperatures below  $T_C$ , the obtained negative magnetoresistance is correlated with the spin-polarized tunneling at the grain boundaries which is determined by the magnetic domain rotation at the grain boundaries. Magnetic coupling between the Co and Mn spin lattices may play a prominent role and the increase of resistivity caused by chemical pressure may lead to negative MR% values [47, 48].

## 4 Conclusion

In summary, we have given a comprehensive analysis of the structural, microstructural, magnetic, and transport properties of the manganite system denoted by the formula  $\text{La}_{2/3}\text{Ca}_{1/3}\text{Mn}_{1-x}\text{Co}_x\text{O}_3$  with  $x = 0.0, 0.1, 0.2,$  and  $0.3$ . The explicit role of the Co substitution with the Mn site has been revealed. Powder X-ray diffraction analysis shows that all systems crystallize in a orthorhombic structure with Pbnm space group. The analysis also demonstrates a slight increase in the lattice parameters with the cobalt substitution. By using SEM analysis, we estimate the average grain sizes which decrease by the amount of Co content from  $1.28 \mu\text{m}$  ( $x = 0.0$ ) to  $0.93 \mu\text{m}$  ( $x = 0.3$ ). The cobalt substitution is found to decrease both the system magnetization and the Curie temperature which are the explicit indicators of the weakening of the double-exchange interaction in the  $\text{Mn}^{3+}\text{-O-Mn}^{4+}$  network. From the transport measurements, the Co substitution is found to increase the resistivity of the samples significantly. Besides, the metal-insulator transition temperature is shown notably decreased by the amount of Co substitution. Approximately, 60% MR value is reported around 190 K for  $x = 0.0$  sample which can be increased or decreased depending on the temperature and the Co content. Specifically, the absolute



MR% values can be higher than 100% as obtained for  $x = 0.3$  sample at low temperatures which promises potential technological applications.

## Acknowledgements

The author would like to acknowledge İbrahim Belenli and Bekir Özçelik for useful discussions and magnetization measurements.

## Compliance with ethical standards

**Conflict of interest** The authors declare that they have no known competing financial interests or personal relationships that could have appeared to influence the work reported in this paper.

## References

1. S.K. Estemirova, V.Y. Mitrofanova, S.A. Uporova, R.I. Gulyaeva, Effect of cation substitution on structural, magnetic and magnetocaloric properties of  $(\text{La}_{0.7}\text{Eu}_{0.3})_{0.75}\text{Sr}_{0.25}\text{Mn}_{0.9}(\text{Me})_{0.1}\text{O}_3$  (Me = Co, Ti). *J. Magn. Magn. Mater.* **502**, 166593 (2020). <https://doi.org/10.1016/j.jmmm.2020.166593>
2. X.G. Chen, J.B. Fu, C. Yun, H. Zhao, Y.B. Yang, H.L. Du, J.Z. Han, C.S. Wang, S.Q. Liu, Y. Zhang, Y.C. Yang, J.B. Yang, Magnetic and transport properties of cobalt doped  $\text{La}_{0.7}\text{Sr}_{0.3}\text{MnO}_3$ . *J. Appl. Phys.* **116**, 103907 (2014). <https://doi.org/10.1063/1.4894713>
3. A. Kumar, C.V. Tomy, A.D. Thakur, Magnetothermopower, magnetoresistance and magnetothermal conductivity in  $\text{La}_{0.95}\text{Sr}_{0.05}\text{Co}_{1-x}\text{Mn}_x\text{O}_3$  ( $0.00 \leq x \leq 1.00$ ). *Mater. Res. Express* **5**, 086110 (2018). <https://doi.org/10.1088/2053-1591/aad44c>
4. I. Troyanchuk, D. Karpinsky, M. Bushinsky, V. Sikolenko, S. Gavrilova, M. Silibin, Magnetic and magnetoresistance properties of  $\text{La}_{0.7}\text{Sr}_{0.3}(\text{Mn}, \text{Co})\text{O}_3$ . *Physica B* **524**, 22–26 (2017). <https://doi.org/10.1016/j.jelechem.2019.05.014>
5. C.O. Ehi-Eromosele, J.A.O. Olugbuyiro, A. Edobor-Osoh, A.A. Adebisi, O.A. Bamgboye, J. Ojeifo, Magneto-structural and antimicrobial properties of sodium doped lanthanum manganite magnetic nanoparticles for biomedical applications: influence of silica coating. *J. Biomim. Biomater. Biomed. Eng.* **37**, 117–127 (2018). <https://doi.org/10.4028/www.scientific.net/jbbbe.37.117>
6. K. Knížek, Z. Jiráček, O. Kaman, M. Maryško, F. Damay, Effect of  $\text{Tb}^{3+}$  doping in mixed-valence manganites and cobaltites. *J. Phys. Condens. Matter* **29**, 405802 (2017). <https://doi.org/10.1088/1361-648X/aa7ff1f>
7. B. Hu, S. Krishnan, C. Liang, S.J. Heo, A.N. Aphale, R. Ramprasad, P. Singh, Experimental and thermodynamic evaluation of  $\text{La}_{1-x}\text{Sr}_x\text{MnO}_{3\pm\delta}$  and  $\text{La}_{1-x}\text{Sr}_x\text{Co}_{1-y}\text{Fe}_y\text{O}_{3-\delta}$  cathodes in Cr-containing humidified air. *Int. J. Hydrog. Energy* **42**, 10208–10216 (2017). <https://doi.org/10.1016/j.ijhydene.2017.01.040>
8. A. Kumar, C.V. Tomy, A.D. Thakur, Magnetothermopower, magnetoresistance and magnetothermal conductivity in  $\text{La}_{0.95}\text{Sr}_{0.05}\text{Co}_{1-x}\text{Mn}_x\text{O}_3$  ( $0.00 \leq x \leq 1.00$ ). *Mater. Res. Express* **5**, 086110 (2018). <https://doi.org/10.1088/2053-1591/aad44c>
9. M.A. Gdaiem, S. Ghodhbane, A. Dhahri, J. Dhahri, E.K. Hlil, Effect of cobalt on structural, magnetic and magnetocaloric properties of  $\text{La}_{0.8}\text{Ba}_{0.1}\text{Ca}_{0.1}\text{Mn}_{1-x}\text{Co}_x\text{O}_3$  ( $x = 0.00, 0.05$  and  $0.10$ ) manganites. *J. Alloys Compd.* **681**, 547 (2016). <https://doi.org/10.1016/j.jallcom.2016.04.143>
10. Y. Moualhi, R. M'nassri, H. Rahmouni, M. Gassoumi, K. Khirouni, Possibility of controlling the conduction mechanism by choosing a specific doping element in a praseodymium manganite system. *RSC Adv.* **10**, 33868 (2020). <https://doi.org/10.1039/d0ra03982a>
11. R. M'nassri, M. Khelifi, H. Rahmouni, A. Selmi, K. Khirouni, N. Chniba-Boudjada, A. Cheikhrouhou, Study of physical properties of cobalt substituted  $\text{Pr}_{0.7}\text{Ca}_{0.3}\text{MnO}_3$  ceramics. *Ceram. Int.* **42**(5), 6145–6153 (2016). <https://doi.org/10.1016/j.ceramint.2016.01.001>
12. A. Selmi, R. M'nassri, W. Cheikhrouhou-Koubaa, N. Chniba-Boudjada, A. Cheikhrouhou, Influence of transition metal doping (Fe Co, Ni and Cr) on magnetic and magnetocaloric properties of  $\text{Pr}_{0.7}\text{Ca}_{0.3}\text{MnO}_3$  manganites. *Ceram. Int.* **41**(8), 10177–10184 (2015). <https://doi.org/10.1016/j.ceramint.2015.04.123>
13. J.C. Debnath, J. Wang, Magnetic and electrical response of Co-doped  $\text{La}_{0.7}\text{Ca}_{0.3}\text{MnO}_3$  manganites/insulator system. *Physica B* **504**, 58–62 (2017). <https://doi.org/10.1016/j.physb.2016.10.017>
14. A. Gómez, E. Chavarriga, J.L. Izquierdo, J. Prado-Gonjal, F. Mompean, N. Rojas, O. Morán, Assessment of the relationship between magneto transport and magnetocaloric properties in nano-sized  $\text{La}_{0.7}\text{Ca}_{0.3}\text{Mn}_{1-x}\text{Ni}_x\text{O}_3$  manganites. *J. Magn. Magn. Mater.* **469**, 558–569 (2019). <https://doi.org/10.1016/j.jmmm.2018.09.036>
15. N. Ibrahim, A.K. Yahya, S.S. Rajput, S. Keshri, M.K. Talari, Double metal–insulator peaks and effect of  $\text{Sm}^{3+}$  substitution on magnetic and transport properties of hole-doped  $\text{La}_{0.85}\text{Ag}_{0.15}\text{MnO}_3$ . *J. Magn. Magn. Mater.* **323**, 2179–2185 (2011). <https://doi.org/10.1016/j.jmmm.2011.03.027>
16. V.S. Kolat, H. Gencer, M. Gunes, S. Atalay, Effect of B-doping on the structural, magnetotransport and magnetocaloric properties of  $\text{La}_{0.67}\text{Ca}_{0.33}\text{MnO}_3$  compounds. *Mater.*

- Sci. Eng. B **140**, 212 (2007). <https://doi.org/10.1016/j.mseb.2007.05.002>
- 17 S. Bharadwaj, A. Tirupathi, N.P. Kumar, S. Pola, Y.K. Lakshmi, Study of magnetic and magnetoresistance behaviour of  $\text{La}_{0.67}\text{Sr}_{0.33}\text{MnO}_3\text{-CoFe}_2\text{O}_4$  composites. *J. Magn. Magn. Mater.* **513**, 167058 (2020). <https://doi.org/10.1016/j.jmmm.2020.167058>
  - 18 M. Eshraghi, P. Kameli, F. Khalili, M.H. Ehsani, H. Salamati, Structural, magnetic and electrical characterization of the  $\text{La}_{0.7}\text{Ca}_{0.3}\text{Co}_{1-x}\text{Mn}_x\text{O}_3$  ( $x=0, 0.7$  and  $1$ ) compounds prepared by a simple method. *J. Rare Earths* **32**, 965 (2014). [https://doi.org/10.1016/S1002-0721\(14\)60170-8](https://doi.org/10.1016/S1002-0721(14)60170-8)
  19. P. Chen, W. He, G. Xiao, J. Wen, T. Yang, X. Wu, T. Wang, Effect of A-site ionic disorder on the structure, magnetic, and magnetocaloric properties of  $\text{La}_{0.7-x}\text{Nd}_x\text{Ca}_{0.3-y}(\text{Ba}, \text{Sr})_y\text{MnO}_3$ . *J. Appl. Phys.* **127**, 055110 (2020). <https://doi.org/10.1063/1.5120740>
  - 20 M. Zhou, Y. Li, I. Jeon et al., Enhancement of low-field magnetoresistance in self-assembled epitaxial  $\text{La}_{0.67}\text{Ca}_{0.33}\text{MnO}_3\text{:NiO}$  and  $\text{La}_{0.67}\text{Ca}_{0.33}\text{MnO}_3\text{:Co}_3\text{O}_4$  composite films via polymer-assisted deposition. *Sci. Rep.* **6**, 26390 (2016). <https://doi.org/10.1038/srep26390>
  21. P. Rivero, V. Meunier, W. Shelton, Electronic, structural, and magnetic properties of  $\text{LaMnO}_3$  phase transition at high temperature. *Phys. Rev. B* **93**, 024111 (2016). <https://doi.org/10.1103/PhysRevB.93.024111>
  22. M.A. Korotin, S.Y. Ezhov, I.V. Solovyev, V.I. Anisimov, D.I. Khomskii, G.A. Sawatzky, Intermediate-spin state and properties of  $\text{LaCoO}_3$ . *Phys. Rev. B* **54**, 5309–5316 (1996). <https://doi.org/10.1103/PhysRevB.54.5309>
  23. G.H. Jonker, J.H. Van Santen, Ferromagnetic compounds of manganese with perovskite structure. *Physica* **16**, 337 (1950). [https://doi.org/10.1016/0031-8914\(50\)90033-4](https://doi.org/10.1016/0031-8914(50)90033-4)
  24. J.H. Van Santen, G.H. Jonker, Electrical conductivity of ferromagnetic compounds of manganese with perovskite structure. *Physica* **16**, 599 (1950). [https://doi.org/10.1016/0031-8914\(50\)90104-2](https://doi.org/10.1016/0031-8914(50)90104-2)
  - 25 C. Zener, Interaction between the d-shells in the transition metals. II. Ferromagnetic compounds of manganese with perovskite structure. *Phys. Rev.* **82**, 403 (1951). <https://doi.org/10.1103/PhysRev.82.403>
  26. A.J. Millis, P.B. Littlewood, B.I. Shraiman, *Phys. Rev. Lett.* **74**, 5144 (1995)
  27. A.J. Millis, B.I. Shraiman, R. Mueller, *Phys. Rev. Lett.* **77**, 175 (1996)
  28. E. Bouzaïene, A.H. Dhahri, J. Dhahri, E.K. Hlil, A. Bajahzar, Effect of A-site-substitution on structural, magnetic and magnetocaloric properties in  $\text{La}_{0.7}\text{Sr}_{0.3}\text{Mn}_{0.9}\text{Cu}_{0.1}\text{O}_3$  manganite. *J. Magn. Magn. Mater.* **491**, 165540 (2019)
  29. S.V. Trukhanov, V.A. Khomchenko, D.V. Karpinsky, M.V. Silibin, A.V. Trukhanov, L.S. Lobanovsky, H. Szymczak, C.E. Botez, I.O. Troyanchuk, A-site ordered state in manganites with perovskite-like structure based on optimally doped compounds  $\text{Ln}_{0.70}\text{Ba}_{0.30}\text{MnO}_3$  ( $\text{Ln} = \text{Pr}, \text{Nd}$ ). *J. Rare Earths* **37**, 1242–1249 (2019). <https://doi.org/10.1016/j.jre.2018.12.010>
  30. P. Gluchowski, R. Nikonkov, R. Tomala, W. Stręk, T. Shulha, M. Serdechnova, M. Zheludkevich, A. Pakalaniškis, R. Skaudžius, A. Kareiva, A. Abramov, A. Kholkin, M.V. Bushinsky, D. Karpinsky, Magnetic properties of  $\text{La}_{0.9}\text{A}_{0.1}\text{MnO}_3$  (A: Li, Na, K) nanopowders and nanoceramics. *Materials* **13**, 1788 (2020). <https://doi.org/10.3390/ma13071788>
  31. A. Ben JaziaKharrat, M. Bourouina, N. Moutia, K. Khirouni, W. Boujelben, Gd doping effect on impedance spectroscopy properties of sol–gel prepared  $\text{Pr}_{0.5-x}\text{Gd}_x\text{Sr}_{0.5}\text{MnO}_3$  ( $0 \leq x \leq 0.3$ ) perovskites. *J. Alloys Compd.* **741**, 723–733 (2018). <https://doi.org/10.1016/j.jallcom.2018.01.236>
  32. A.I. Kurbakov, V.A. Ryzhov, V.V. Runov, E.O. Bykov, I.I. Larionov, V.V. Deriglazov, C. Martin, A. Maignan, Study of phase separation phenomena in half-doped manganites with isovalent substitution of rare-earth cations on example of  $\text{Sm}_{0.32}\text{Pr}_{0.18}\text{Sr}_{0.5}\text{MnO}_3$ . *Phys. Rev. B* **100**, 184424 (2019). <https://doi.org/10.1103/PhysRevB.100.184424>
  33. A. Anand, R.K. Veena, M. Manjuladevi, V.S. Veena, S. Yuri, S. Sagar, *J. Magn. Magn. Mater.* **471**, 537 (2019). <https://doi.org/10.1016/j.jmmm.2018.09.062>
  - 34 N. Mahamdioua, A. Amira, S.P. Altintas, A. Saoudeh, Y. Boudjadja, L. Amirouche, A. Varilci, C. Terzioglu, Structural and magneto-transport properties of copper doped double layered manganites  $\text{La}_{1.4}\text{Ca}_{1.6}\text{Mn}_2\text{O}_7$ . *J. Supercond. Nov. Magn.* **26**, 1441–1444 (2013). <https://doi.org/10.1007/s10948-012-2024-0>
  35. K. Ghosh, S.B. Ogale, R. Ramesh, R.L. Greene, T. Venkatesan, K.M. Gapchup, R. Bathe, S.I. Patil, Transition-element doping effects in  $\text{La}_{0.7}\text{Ca}_{0.3}\text{MnO}_3$ . *Phys. Rev. B* **59**, 533 (1999). <https://doi.org/10.1103/PhysRevB.59.533>
  - 36 A. Kumar, C.V. Tomy, A.D. Thakur, Magnetothermopower, magnetoresistance and magnetothermal conductivity in  $\text{La}_{0.95}\text{Sr}_{0.05}\text{Co}_{1-x}\text{Mn}_x\text{O}_3$  ( $0.00 \leq x \leq 1.00$ ). *Mater. Res. Express* **5**, 086110 (2018). <https://doi.org/10.1088/2053-1591/aad44c>
  37. V. Petricek, M. Dusek, L. Palatinus, Crystallographic computing system JANA2006: general features. *Z. Kristallogr.* **229**(5), 345–352 (2014). <https://doi.org/10.1515/zkri-2014-1737>
  38. R. Jia et al., Crossover effect of inter-granular transport and quantum correction in Co-doping  $\text{La}_{2/3}\text{Ca}_{1/3}$

- $\text{MnO}_3$  manganites. *J. Magn. Magn. Mater.* **329**, 65–7066 (2013). <https://doi.org/10.1016/j.jmmm.2012.09.021>
39. C. Suryanarayan, M. Grant Norton, *X-Ray Diffraction: A Practical Approach* (Plenum Press, New York, 1998). <https://doi.org/10.1007/978-1-4899-0148-4>
40. R.F. Klie, J.C. Zheng, Y. Zhu, M. Varela, J. Wu, C. Leighton, Direct measurement of the low-temperature spin-state transition in  $\text{LaCoO}_3$ . *Phys. Rev. Lett.* **99**, 047203 (2007). <https://doi.org/10.1103/PhysRevLett.99.047203>
41. R.D. Shannon, Revised effective ionic radii and systematic studies of interatomic distances in halides and chalcogenides. *Acta Crystallogr. A* **32**, 751 (1976). <https://doi.org/10.1107/S0567739476001551>
42. C.A. Schneider, W.S. Rasband, K.W. Eliceiri, NIH Image to ImageJ: 25 years of image analysis. *Nat. Methods* **9**, 671–675 (2012). <https://doi.org/10.1038/nmeth.2089>
43. K.Y. Wang, W.H. Song, J.M. Dai, S.L. Ye, S.G. Wang, Structural, magnetic, and transport properties in a Cu-doped  $\text{La}_{0.7}\text{Ca}_{0.3}\text{MnO}_3$  system. *J. Appl. Phys.* **90**, 6263 (2001). <https://doi.org/10.1063/1.1415757>
44. S. Surthi, S. Kotru, R.K. Pandey, P. Fournier, Double-peak resistivity transport properties of  $\text{La}_{0.67}\text{Ca}_{0.33}\text{MnO}_3$  ceramics. *Solid State Commun.* **125**, 107–110 (2003). [https://doi.org/10.1016/S0038-1098\(02\)00705-6](https://doi.org/10.1016/S0038-1098(02)00705-6)
45. P. Perna, D. Maccariello, F. Ajejas, R. Guerrero, L. Méchin, S. Flament, J. Santamaria, R. Miranda, J. Camarero, Engineering large anisotropic magnetoresistance in  $\text{La}_{0.7}\text{Sr}_{0.3}\text{MnO}_3$  films at room temperature. *Adv. Funct. Mater.* **27**, 1700664 (2017). <https://doi.org/10.1002/adfm.201700664>
46. R. Lukose, N. Zurauskiene, V. Stankevicius et al., Room temperature Co-doped manganite/graphene sensor operating at high pulsed magnetic fields. *Sci. Rep.* **9**, 9497 (2019). <https://doi.org/10.1038/s41598-019-46012-2>
47. X.X. Zhang, J.M. Hernandez, Observation of colossal positive and negative magnetoresistance in perovskite-type manganese oxide  $\text{Nd}_{0.67}\text{Ca}_{0.33}\text{MnO}_3$ . *Europhys. Lett.* **47**(4), 487–493 (1999). <https://doi.org/10.1209/epl/i1999-00414-0>
48. Y.N. Kim, S.J. Kim, E.K. Lee, E.O. Chi, N.H. Hur, C.S. Hong, Large magnetoresistance in three dimensionally ordered macroporous perovskite manganites prepared by a colloidal templating method. *J. Mater. Chem.* **14**, 1774 (2004). <https://doi.org/10.1039/B402899F>

**Publisher's Note** Springer Nature remains neutral with regard to jurisdictional claims in published maps and institutional affiliations.